Supplementary Materials for

Accelerated actin filament polymerization from microtubule plus-ends

Jessica L. Henty-Ridilla, Aneliya Rankova, Julian A. Eskin, Katelyn Kenny, and Bruce L. Goode

correspondence to: goode@brandeis.edu

This PDF file includes:

Materials and Methods
Figs. S1 to S9
Figure Legends S1 to S9
Captions for Movies S1 to S11

Other Supplementary Materials for this manuscript includes the following:

Movies S1 to S11

Materials and Methods

Reagents

Except where noted, all reagents were purchased from Sigma-Aldrich, St. Louis, MO.

Plasmid construction

Full-length CLIP-170-1 (NCBI: NP_001234926.1) and its sub-fragments were PCR amplified from a cDNA plasmid (MHS6278-211689129) (GE Dharmacon, Lafayette, CO) and sub-cloned into the BamHI and NotI sites of a modified pRS426 (*URA3,* 6×His, *GAL1/10*) yeast expression vector (*37*). To generate CLIP-170-2 (NCBI: NP_002947.1) and CLIP-170-3 (NCBI: NP_937883.1) isoforms, we internally deleted sequences from CLIP-170-1 by site-directed mutagenesis (see Fig. S1). FEED1 (CLIP-170-1$^{VEEE445\text{-}448AAAA}$) and FEED2 (CLIP-170-1$^{ITKGDLE450\text{-}456AAAAAAA}$) mutants were also generated by site-directed mutagenesis. To build a yeast expression plasmid for SNAP-FL-CLIP-170-1, the ORF was excised using BamHI and NotI and subcloned into the same sites of pCG105, a modified pRS426 (*URA3,* 6×His, *GAL1/10*) with N-terminal 6×His and SNAP tags (*24*). The pSuper-shRNA (Thermo Fisher Scientific) against CLIP-170 was generated following the manufacturer's protocol and a previously characterized targeting sequence (*16*). CLIP-170 rescue constructs for mammalian expression were PCR amplified from pCG105 and sub-cloned using BamHI and EcoRI sites into the mCherry-C1 vector (Clonetech Laboratories Inc., Mountain View, CA). For purification of full-length EB1, the ORF was PCR amplified from pGFP-EB1 (Addgene plasmid #17234) and sub-cloned into pGEX-6p1 using BamHI and NotI sites.

Protein purification

Proteins were purified and/or modified as described: rabbit skeletal muscle actin (RMA) (*38*), biotinylated RMA (*24*), N-(1-pyrenyl) iodoacetamide-labeled (pyrene) RMA (*39*), Oregon Green (OG)-labeled RMA (*22*), bovine tubulin (*40*), AlexaFluor647 bovine tubulin (*41*), GMP-CPP MT seeds (*41*), SNAP-mDia1 FH1-FH2-tail (553-1255) (*24*), mDia1 FH1-FH2-tail (553-1255) (*25*), mDia1 FH2-tail (739-1255) (*42*), mDia1ΔCT (549-1200) (*23*) (SDS-PAGE gels of purified mDia1 polypeptides in Figure S7), mDia2 FH1-FH2-tail (*32*), human Daam1 FH1-FH2-tail (*37*), human profilin (*13*), and human Capping Protein (CP) (*43*).

6×His-tagged CLIP-170 proteins (full-length, mutants, and fragments) were purified from *S. cerevisiae* as follows (SDS-PAGE gels shown in Figure S9). Briefly, plasmids were transformed into yeast strain BJ2168 and 2 L of cells were grown at 25°C to late log phase (OD_{600} = 0.8) in selective media containing 2% raffinose (Gold Biotechnology, St. Louis, MO). Expression was induced for 12-16 h by addition of 2% galactose (Gold Biotechnology), 20 g bacto-peptone (US Biological, Salem, MA), and 10 g yeast extract (US Biological). Yeast cells were harvested by centrifugation and resuspended in a 0.2:1 v/w ratio of water, mechanically lysed in a coffee grinder in liquid N_2 and stored at -80 °C. For each purification, 10 g of frozen yeast powder was resuspended 1:1 (w/v) in 30 mM imidazole (pH 8.0), 2× PBS (pH 7.4), 1% Nonidet P-40, 0.5 mM DTT, complete protease inhibitor cocktail (Roche, Branford, CT), and 2 mM phenylmethylsulfonyl fluoride (PMSF). The lysate was cleared for 30 min at 300,000 × *g*, and the supernatant was mixed with 0.3 mL of Ni^{2+}-NTA-agarose beads (Qiagen, Valencia, CA) for

2 h at 4 °C. Beads were washed three times in high-salt buffer (30 mM imidazole, PBS with 350 mM NaCl, and 0.5 mM DTT) and an additional three times in low-salt buffer (50 mM imidazole, PBS, and 0.5 mM DTT), then proteins were eluted in PBS supplemented with 350 mM imidazole and 0.5 mM DTT. Proteins were desalted on a Superose 6 gel filtration column (GE Healthcare, Pittsburgh, PA) or PD-10 columns (GE Healthcare) equilibrated in $HEKG_5$ (20 mM HEPES pH 7.5, 1 mM EDTA, 50 mM KCl, 5% glycerol, and 1 mM DTT). Peak fractions were pooled, concentrated in Amicon Ultra centrifugal concentrators (Millipore, Bedford, MA), aliquoted, flash-frozen in liquid N_2, and stored at -80 °C. SNAP-tagged proteins were fluorescently labeled while still bound to beads during purification, directly after the low-salt wash, by incubation overnight at 4 °C with 25 μM SNAP-Surface 488, 549, or 649 dyes (NEB, Ipswich, MA). Beads were then washed five times to remove excess dye, and proteins were eluted, concentrated, aliquoted, and stored as above. GST-EB1 was transformed into the *E. coli* BL21(DE3) strain, and 2 L of cells were grown to OD_{600} = 0.8 in Terrific Broth. Protein expression was induced for 16 h at 18 °C with 0.4 mM IPTG. Cells were harvested by centrifugation, flash frozen and stored at -80 °C. Cell pellets was resuspended in lysis buffer (50 mM Tris pH 8.0, 150 mM NaCl, 1 mM EDTA pH 8.0, 1 mM DTT, complete protease inhibitor cocktail) and lysed by sonication. Lysates were cleared for 25 min at 33,500 × g, and the harvested supernatant was mixed with 0.3 mL of glutathione-agarose beads (Thermo Fisher Scientific, Pittsburgh, PA) for 2 h at 4 °C. Beads were washed five times with wash buffer (50 mM Tris pH 8.0, 150 mM NaCl, 1 mM EDTA pH 8.0, 1 mM DTT) and the GST-tag was cleaved using 20 U PreScission Protease (GE Healthcare) overnight at 4 °C. Proteins were desalted using PD-10 columns equilibrated in $HEKG_5$, and stored as above.

Protein concentrations were determined by band densitometry on Coomassie-stained SDS-PAGE gels, compared to BSA standards. For SNAP-tagged proteins, percent labeling was determined using the following fluorophore absorbance and extinction coefficients: SNAP-Surface Alexa Fluor 488: ε496 = 73,000 M^{-1} cm^{-1}, SNAP-Surface 549: ε560 = 140,300 M^{-1} cm^{-1}; SNAP-Surface 649: ε655 = 250,000 M^{-1} cm^{-1}. SNAP-448-mDia1, SNAP-649-mDia1, and SNAP-549-FL-CLIP-170-1 proteins were 32%, 65% and 69% labeled, respectively.

Total internal reflection fluorescence (TIRF) microscopy

Glass coverslips (24 × 60 mm #1.5; Thermo Fisher Scientific) were sonicated for 1 h in 2% Micro-90 detergent, followed by 1 h sonication in 100% ethanol, then 30 min sonication in 0.1 M KOH and $_{dd}H_2O$, respectively. Then coverslips were sonicated in 100% ethanol for 1 hr, rinsed 10 times with $_{dd}H_2O$ and sonicated for an additional 20 min in $_{dd}H_2O$. Cleaned coverslips were stored in 100% ethanol before use. Prior to imaging, each coverslip was rinsed with $_{dd}H_2O$, dried with N_2, coated by applying 110 μL of 2 mg/mL methoxy-poly(ethylene glycol) (mPEG)-silane MW 2,000 and 2 μg/mL biotin-PEG-silane MW 3,400 (Laysan Bio, Arab, AL) in 80% ethanol (pH 2.0) and incubated for 16 h at 70 °C. Flow cells were assembled by rinsing PEG-coated coverslips 6 times with $_{dd}H_2O$, drying with N_2, and adhering to μ-Slide $VI^{0.1}$ (0.1 mm × 17 mm × 1 mm) flow chambers (Ibidi, Martinsried, Germany) with double-sided tape (2.5 cm × 2 mm × 120 μm) and five-minute epoxy resin (Devcon, Riviera Beach, FL).

Flow cells were sequentially conditioned with the following filter-sterilized buffers for 30 s each: 1% BSA, 4 μg/mL streptavidin in 10 mM Tris-HCl (pH 8.0), 1% BSA, and TIRF buffer. Actin TIRF reactions were initiated by adding 1 μM G-actin (10% OG-labeled and 0.2% biotinylated) to premixed proteins in actin TIRF buffer (10 mM imidazole (pH 7.4), 50 mM KCl, 1 mM $MgCl_2$, 1 mM EGTA, 0.2 mM ATP, 10 mM DTT, 15 mM glucose, 20 μg/mL catalase, 100 μg/mL glucose oxidase, 1% BSA, and 0.25% methyl cellulose [4000 cP]). Time lapse TIRF imaging was performed using a Ti200 inverted microscope (Nikon Instruments, New York, NY) equipped with three 100 mW solid-state lasers (emission 488 nm, 543 nm, and 633 nm; Agilent Technologies, Santa Clara, CA), a CFI Apo 60× 1.49 N.A. oil-immersion TIRF objective (Nikon Instruments), and an EMCCD camera with a pixel size of 0.267 μm (Andor Ixon, Belfast, Northern Ireland). Focus was maintained using the Perfect Focus System (Nikon Instruments). For single-color movies of OG-actin filaments, frames were captured every 5 s (80 ms, 488 nm excitation). For multi-wavelength movies, images were captured every 3 s in series: 80 ms, 488 nm excitation; 100 ms, 543 nm excitation; and 100 ms, 633 nm excitation. All lasers were used at 10% power. For imaging MTs, or MTs and actin together, images were captured every 5 s in series: 80 ms, 488 nm excitation; 100 ms, 543 nm excitation; and 100 ms, 633 nm excitation. All lasers were used at 10% power. Reactions were introduced into the flow chamber, which was then mounted on the microscope stage. Flow-through was achieved using a controlled syringe pump (Harvard Apparatus, Holliston, MA). Time between initial mixing of proteins and the start of TIRF recording was typically 20-30 s.

For TIRF reactions containing dynamic MTs or dynamic MTs and actin filaments, the following adjustments were made. To monitor CLIP-170 and mDia1 interactions with dynamic MTs (without actin present), TIRF was performed as above except that instead of TIRF buffer we used BRB80 (80 mM PIPES, 1 mM $MgCl_2$, 1mM EGTA, 10 mM DTT, 0.1 mM GTP, 0.1 mM ATP, 15 mM glucose, 20 μg/mL catalase, 100 μg/mL glucose oxidase, 1% BSA, and 0.25% methyl cellulose [4000 cP]; pH 6.8 with KOH). Reactions were performed at 35 °C, maintained by a stage heater (Ibidi) and an objective heater (Andor Technology, Windsor, CT). GMP-CPP MT seeds were added to the TIRF chamber and tethered to the surface via an avidin-biotin conjugation system. Then the chamber was washed with BRB80 buffer, and 15 μM tubulin (30% Alexa Fluor 649 labeled) and other premixed proteins were flowed in. Conditions were similar for MT-actin co-reconstitution assays, except that the final ingredients also included 1 μM G-actin (10% OG-labeled and 0.2% biotinylated). In both cases (MTs alone, or MTs and actin), images were acquired at 5 s intervals and analyzed in Fiji (*44*).

Quantitative image analysis

Background fluorescence was removed from each time series using the background subtraction tool (rolling ball radius, 20 pixels) in Fiji. A 0.5-pixel Gaussian blur was applied to all montages and time-lapse images. Minimal contrast enhancement or changes to the black level were applied to the entire stack to improve image quality for analysis and display. Mean fluorescence intensity was calculated in Fiji from time-lapse TIRF movies. Linear regression and 95% confidence intervals were calculated in GraphPad Prism version 6.0c (GraphPad Software, La Jolla, CA). Nucleation was quantified by counting the number of filaments per $(100\ \mu m)^2$ from $n \geq 9$ fields of view 200 s after initiating actin assembly. Elongation rates were quantified by measuring

filament length every frame using the segmented line tool in Fiji, plotting length versus time, then fitting the data with a linear regression. The rate is the slope from the line of best fit. Conversion of elongation rates from measured polymer lengths to subunits s^{-1} assumes 370 actin subunits per micron of filament (*45*) and 1625 tubulin dimers per micron of MT polymer (*46*).

For single molecule colocalization analysis, biotinylated SNAP-649-mDia1 molecules were tethered to the coverglass surface, and then 25 nM SNAP-549-CLIP-170-1 with or without the indicated concentrations of unlabeled CLIP-170-$1^{348-460}$ fragment in TIRF buffer were flowed in. After 5 min, co-localization of mDia1 with CLIP-170-1 was measured.

Step photobleaching analysis was performed on passively adsorbed SNAP-549-CLIP-170 molecules in TIRF buffer lacking glucose oxidase or catalase as described (*24*). Surface-adsorbed molecules were subjected to constant illumination at high laser power (80%, 100 mW) and imaged every 0.1 s. Background fluorescence was subtracted as above, and fluorescence intensities of molecules were measured in Fiji. Stepwise reductions in the integrated fluorescence intensities over time were scored and the oligomeric state of SNAP-549-CLIP-170 was determined by comparing the distribution of number of photobleaching events to the probability distribution of the number of fluorescent subunits calculated from the binomial distribution, as described (*24*).

To quantify mean duration of uncapped growth (Fig. 2G & 2H), filament length traces (20 min observation window) in the presence of different concentrations of CLIP-170-1 were scored for pauses in elongation (defined as no growth for ≥ 3 consecutive frames, or 15 s), and the durations of the pauses were measured and averaged ($n > 300$). Data were fit to a curve using the Michaelis-Menten equation; $R^2 = 0.955$.

Cell culture, transfection, and image analyses

Cortical neurons were isolated from E18 rat pups and cultured on a confluent layer of glia on glass coverslips in 24-well tissue culture dishes as described (*47*). Briefly, 2 day in vitro (DIV) neurons were transfected using the calcium phosphate method (*48*) with 200 ng pCMV-GFP plasmid and either 100 ng control pSUPER plasmid carrying a scrambled shRNA or shCLIP-170 pSUPER plasmid carrying an shRNA against CLIP-170 (*16*). For rescues, cells were co-transfected with mChr-C1 plasmid expressing RNAi-resistant full-length wild type or FEED1 mutant CLIP-170-1. For experiments in which we expressed full-length CLIP-170-1 (wild type or FEED1 mutant) without silencing endogenous CLIP-170 (Fig. 4C & 4D), we omitted the shRNA plasmids. Transfection efficiency by this method in neurons is approximately 10%, with 93% of transfected neurons obtaining both plasmids (*47*). Neurons were fixed at 4-5 DIV in 4% paraformaldehyde and 4% sucrose to visualize dendrite morphology by cytosolic GFP signal. All experiments were performed in two or more trials using neurons prepared from separate batches of rats.

Neurons were imaged using a 3i Marianas spinning disk confocal system (Intelligent Imaging Innovations, Denver, CO), consisting of a Zeiss Observer Z1 microscope equipped with a 100

mW solid-state laser emission 488 nm, a 63× plan apochromat objective (N.A. 1.4), a Yokagawa CSU-X1 confocal head, and a QuantEM 512SC EMCCD camera. Image acquisition and quantification was performed using Slidebook 6.0 (3i, Inc) and Fiji in a single-blind manner with identical settings for laser power, acquisition and z-stack (10 optical sections with 0.5 um step size). Sholl analysis was performed using a Fiji plugin by measuring the mean the number of dendrite crossings through a series of 11 concentric circles of increasing radii (10 μm intervals) centered on the cell body.

The ability of the pSUPER shCLIP-170 plasmid to knockdown endogenous CLIP-170 was tested in the mouse Neuroblastoma cell line (N2A). Cells were grown in DMEM (Thermo Fischer Scientific) supplemented with 200 mM L-glutamine (Thermo Fisher Scientific) and 10% FBS. Transfections were performed using Lipofectamine 3000 according to manufacturers instructions (Thermo Fisher Scientific) in 6-well plates, using 77,000 cells and 200 ng plasmid per well. Transfection efficiencies were > 80%. After 48 h, cells were lysed in lysis buffer (20 mM Tris pH 7.4, 0.5 % Triton X-100, and 150 mM NaCl) for 30 min at 4 °C. CLIP-170 levels were measured by Western blotting, loading 20 μg total cell lysate per lane (measured by Bradford Assay against a BSA standard curve). Blots were probed with rabbit primary antibody CLIP-170 H3 (Santa Cruz Biotechnology, Dallas, TX) and donkey anti-rabbit secondary antibody IRDye 680RD 926-68073 (Licor, Lincoln, NE). Bands were quantified using an Odyssey infrared imaging system (Licor).

Live-cell imaging in N2A cells was done using TIRF microscopy. Cells were transfected as above except with 100 ng of plasmid (GFP-EB1 and mChr-CLIP-170-1 or mChr-FEED1) in 6-well plates. After 24 h, cells were replated on glass-bottom dishes and imaged after another 5 h. Imaging was performed in RPM1 buffer (Thermo Fischer Scientific) supplemented with 20 mM HEPES (pH 7.4), 10% FBS, 20 mM L-glutamine, and 1 mM sodium pyruvate (Thermo Fischer Scientfic) and 100 ng of 652-Sir-Tubulin (Cytoskeleton, Denver, CO). Individual dishes were imaged for a maximum of 30 min. In each condition, localization of EB1 and CLIP-170 was scored on MT ends from 300 kymographs drawn at the periphery of cells (10 kymographs for each of 30 cells). Mean velocity, mean lifetime, and mean dynamicity of GFP-EB1 or mChr-CLIP-170 and mChr-FEED1 comets on the ends of MTs were calculated using plusTipTracker in utrack software (Version 2.1.3) (*36*) in Matlab (version R2015a). Each data point in the graphs (Fig. 4G and Fig. S8E) is the mean of thousands of comets from one cell.

Bulk actin assembly assays

Bulk actin assembly assays were performed as described (*24*, *37*). Briefly, 2 μM monomeric RMA (5% pyrene labeled) in G-buffer (10 mM Tris-HCl (pH 8.0), 0.2 mM ATP, 0.2 mM $CaCl_2$, and 0.2 mM DTT) was recycled to Mg-ATP-actin immediately before each reaction. Actin was rapidly mixed with proteins or control buffer supplemented with initiation mix (2 mM $MgCl_2$, 0.5 mM ATP, 50 mM KCl), and fluorescence was monitored at excitation 365 nm and emission 407 nm at 25 °C in a fluorimeter (Photon Technology International, Lawrenceville, NJ). For reactions in Fig. S5A & S5B, CP and buffer or CP and CLIP-170-1 was spiked in at 100 s.

Data analysis

Actin filament elongation rates fell into two distinct subpopulations in reactions containing formins, and three subpopulations in reactions containing both formins and CLIP-170. To test whether the average elongation rate for a subpopulation was significantly different from that of another (designated) subpopulation in a control reaction, a Mann-Whitney test was performed. Statistical tests for significance (Mann-Whitney and Student's *t*-test), as well as linear and nonlinear regressions were performed in GraphPad Prism version 6.0c (GraphPad Software, La Jolla, CA). For Sholl analysis in primary neurons, an ANOVA test was performed using GraphPad Prism version 6.0c to determine significant differences between treatments.

Figure S1.

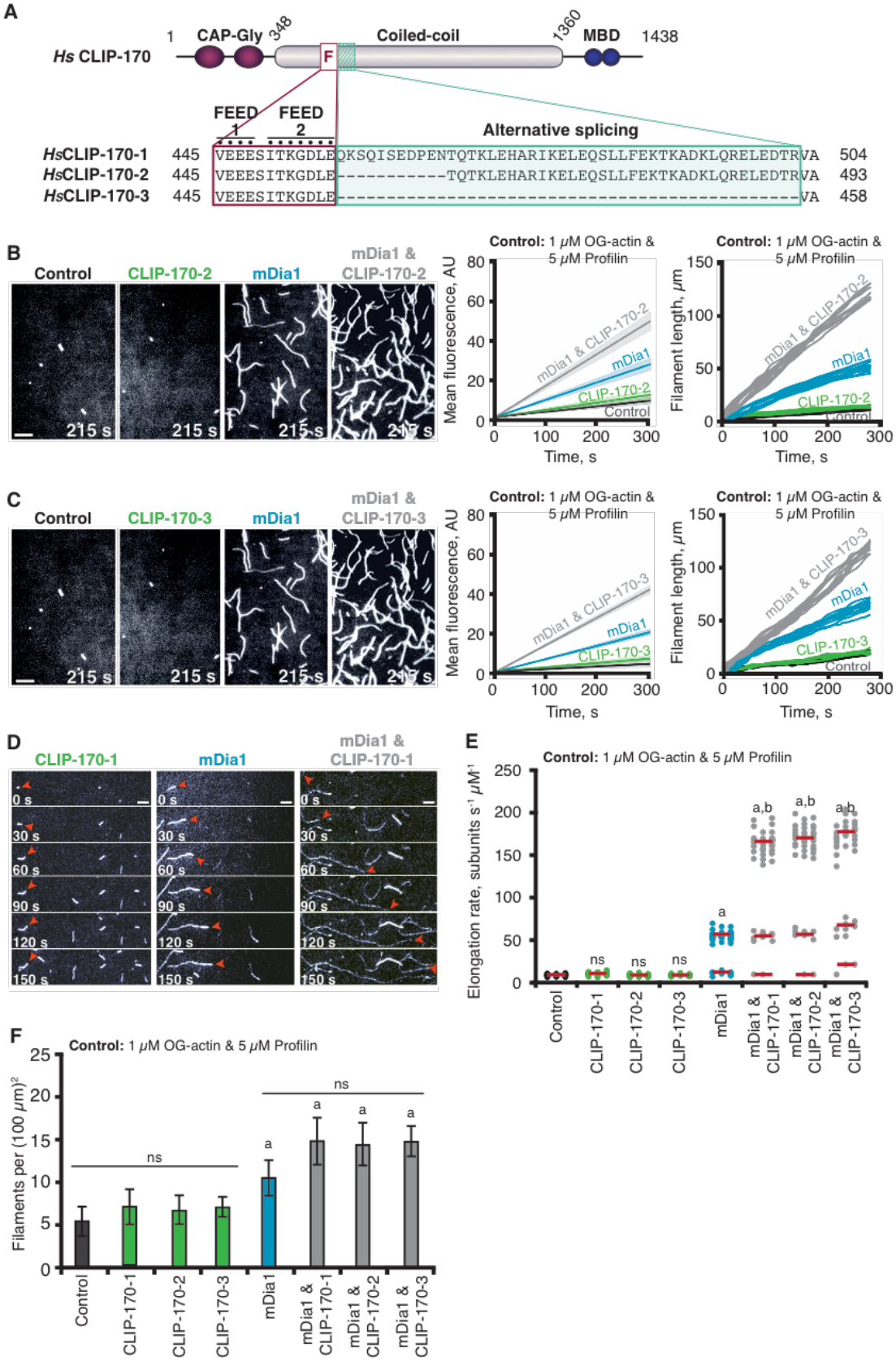
A
Hs CLIP-170
1
CAP-Gly
348
Coiled-coil
1360
MBD
1438
F
FEED 1
FEED 2
Alternative splicing
HsCLIP-170-1 445 VEEESITKGDLEQKSQISEDPENTQTKLEHARIKELEQSLLFEKTKADKLQRELEDTRVA 504
HsCLIP-170-2 445 VEEESITKGDLE----------TQTKLEHARIKELEQSLLFEKTKADKLQRELEDTRVA 493
HsCLIP-170-3 445 VEEESITKGDLE--VA 458
B
Control
CLIP-170-2
mDia1
mDia1 & CLIP-170-2
215 s
Control: 1 μM OG-actin & 5 μM Profilin
Mean fluorescence, AU
Filament length, μm
Time, s
C
Control
CLIP-170-3
mDia1
mDia1 & CLIP-170-3
D
CLIP-170-1
mDia1
mDia1 & CLIP-170-1
0 s
30 s
60 s
90 s
120 s
150 s
E
Elongation rate, subunits s-1 μM-1
ns
a
a,b
F
Filaments per (100 μm)2
Control
CLIP-170-1
CLIP-170-2
CLIP-170-3
mDia1
mDia1 & CLIP-170-1
mDia1 & CLIP-170-2
mDia1 & CLIP-170-3

Fig. S1. Comparison of each CLIP-170 splice isoform on mDia1-mediated actin assembly. **(A)** Schematic of CLIP-170 isoforms highlighting the FEED sequence (F), FEED1 (^{445}VEEE/AAAA^{448}) and FEED2 (^{450}ITKGDLE/AAAAAAA^{456}) mutants, and the alternatively spliced region (teal). **(B-C)** Representative images from TIRF experiments. Left panels show images from TIRF movies 215 s after initiation of actin assembly. All reactions contain 1 μM G-actin (10% OG-labeled; 0.2% biotin-actin) and 5 μM profilin. Variable components: 50 pM mDia1 (FH1-FH2-tail) and 25 nM full-length CLIP-170-2 or CLIP-170-3. Scale bars, 20 μm. Middle panels show graphs of total actin polymer mass over time, averaged from the fluorescence intensity in multiple fields of view ($n \geq 3$); linear curve fits plotted. Shading indicates 95% confidence intervals for each condition. Right panels show graphs with representative actin filament length traces from TIRF movies, plotted at 10 s intervals. **(D)** Representative actin filaments elongating at different rates in TIRF reactions that contain the proteins indicated, concentrations as in (B-C). **(E)** Distributions of filament elongation rates from TIRF reactions as in (B-C), comparing the effects of 25 nM of each CLIP-170 isoform. For each condition, rates were measured for 50 filaments in each of three independent experiments (n = 150). Red bars are average elongation rates for filament subpopulations, measured from all 150 filaments. For simplicity, distributions of rates are only shown from one experiment (n = 50). **(F)** Average number of filaments visible after 200 s in TIRF reactions as in (B-C). Data were quantified from three separate fields of view for each of three independent experiments (n = 9). Error bars, SE. Statistical differences: ns, not significantly different from control; a, significantly different compared to control ($p < 0.05$); b, compared to control containing formin ($p < 0.05$).

Figure S2.

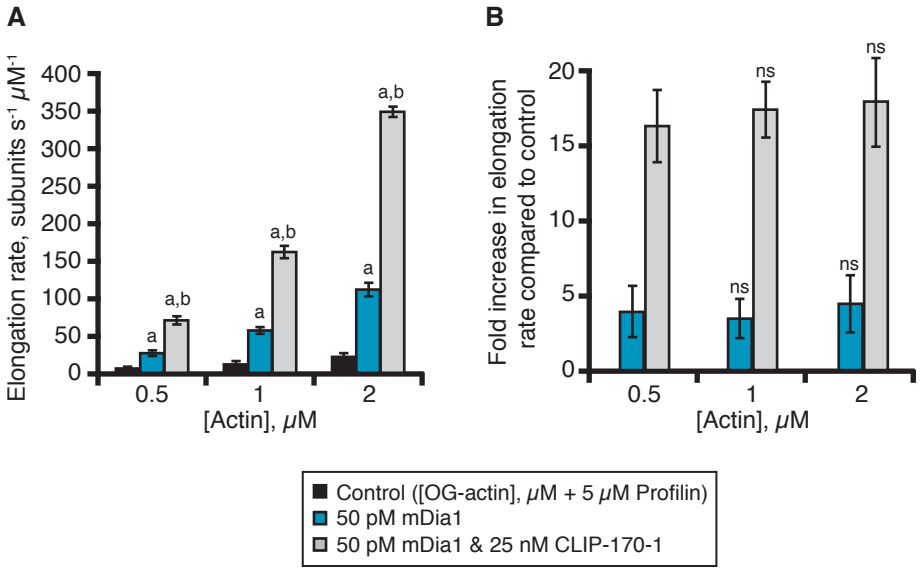

Fig. S2. Actin concentration effects on CLIP-170-mDia1-mediated actin filament elongation.

(A) Mean filament elongation rates (n = 150) measured from TIRF reactions containing 5 μM profilin and variable concentrations of G-actin (10% OG-labeled; 0.2% biotin-actin), with or without 50 pM formin (mDia1 FH1-FH2-tail) and 25 nM CLIP-170-1. Statistical differences: ns, not significantly different from control; a, significantly different compared to control ($p < 0.05$); b, compared to formin control ($p < 0.05$). Error bars, SE. **(B)** Fold increase in rate of mDia1-mediated actin filament elongation stimulated by CLIP-170-1 at different actin monomer concentrations, calculated from the data in (A). Error bars, SE. Fold effects of CLIP-170-1 on elongation were not significantly different at the three different actin concentrations.

Figure S3.

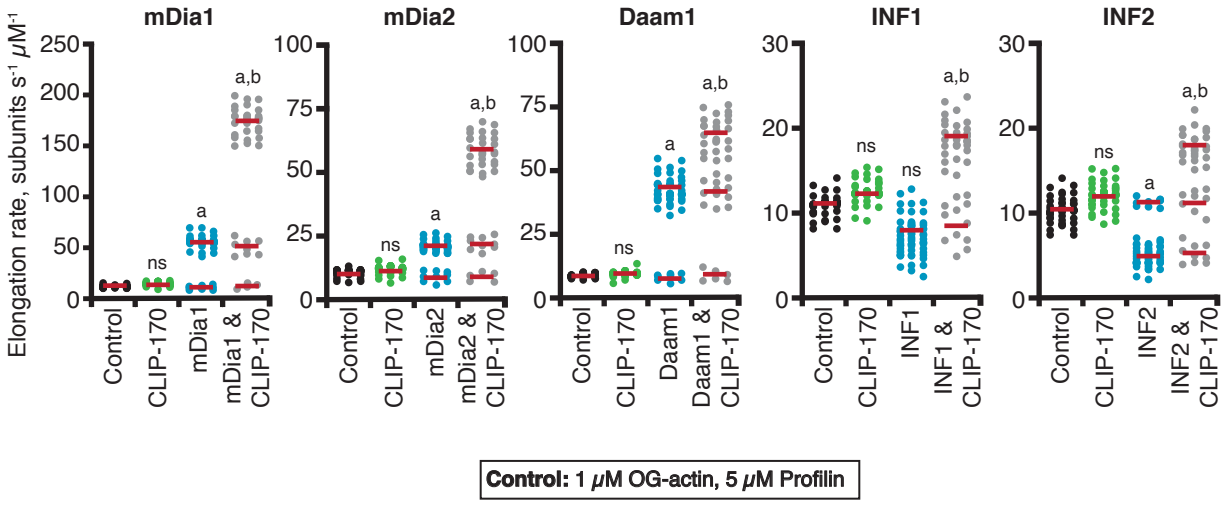

Fig. S3. CLIP-170 effects on actin filament elongation mediated by different formins. Filament elongation rates measured from TIRF reactions containing 1 µM G-actin (10% OG-labeled; 0.2% biotin-actin), 5 µM profilin, with or without 25 nM CLIP-170-1, and with or without each formin (FH1-FH2-tail) indicated. mDia1, mDia2, and Daam1 were used at 50 pM, whereas INF1 and INF2 were used at 100 nM because they are weaker nucleators (*32*). For each condition, rates were measured for 50 filaments in each of three independent experiments (n = 150). Red bars are average elongation rates for subpopulations, measured from all 150 filaments. For simplicity, distributions of rates are only shown from one experiment (n = 50). Statistical differences: ns, not significantly different from control; a, significantly different compared to control ($p < 0.05$); b, compared to control containing formin ($p < 0.05$).

Figure S4

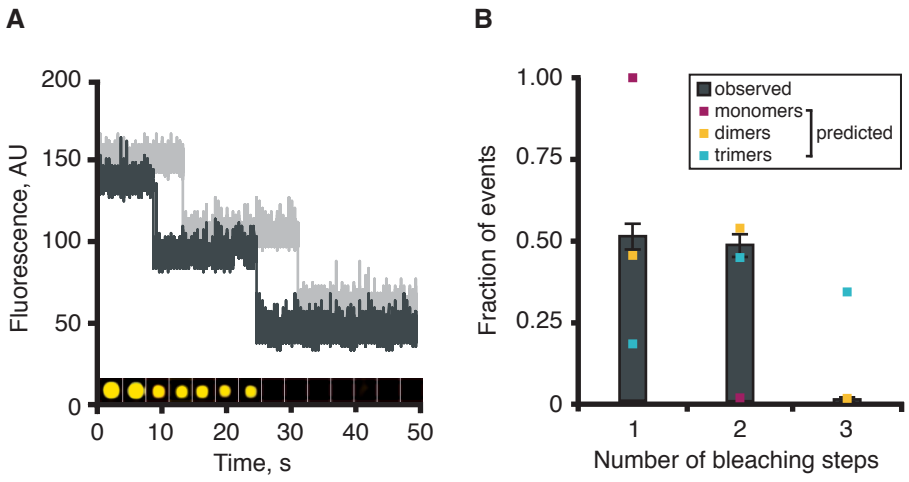

Fig. S4. Oligomerization state of fluorescently-labeled CLIP-170-1.
(A) Step photobleaching analysis of surface-adsorbed SNAP-549-CLIP-170-1 molecules. Fluorescence intensity over time is shown for two representative dimers. Bottom inset (2 × 2 μm) shows raw images for a single two-step bleaching event. **(B)** Distribution of observed number of bleaching events (n = 300) (grey bars) and the predicted number of bleaching events (squares) for different oligomeric states (color-coded), calculated using the measured labeling stoichiometry (0.69 dye per SNAP-CLIP-170-1 monomer). Error bars, SE.

Figure S5.

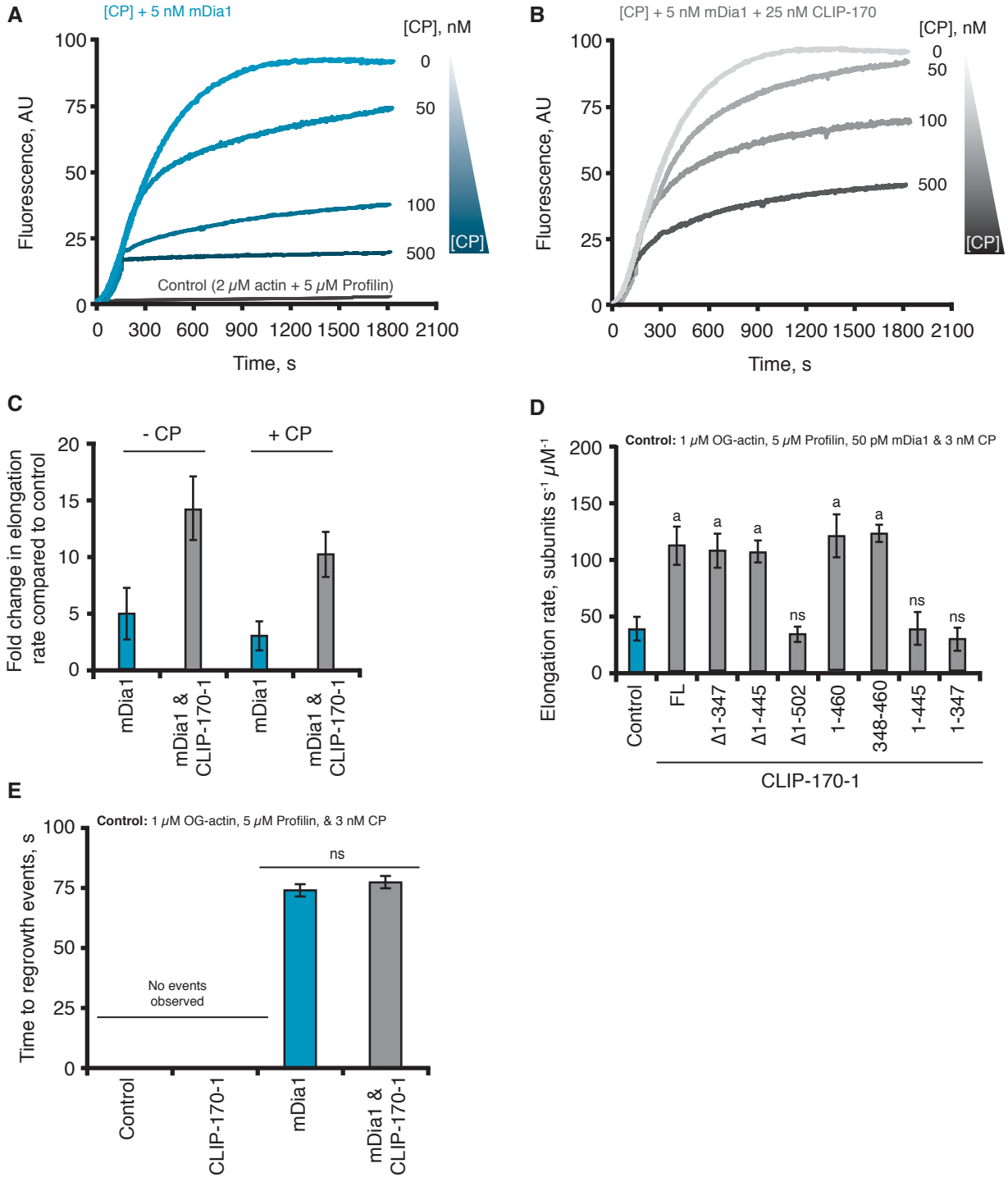

Fig. S5. Effects of CLIP-170-1 on duration of mDia1-mediated actin filament elongation in the presence of Capping Protein (CP).

(A-B) Bulk fluorescence assays comparing the rates of actin assembly in the presence of different concentrations of CP stimulated by mDia1 (A) or mDia1 and CLIP-170-1 (B). Actin

assembly was initiated at time zero with mDia1 present, and after 100 s, CP with or without CLIP-170-1 was spiked in. All reactions contain 2 μM G-actin (5% pyrene-labeled) and 5 μM profilin. Variable components: 5 nM mDia1 (FH1-FH2-tail), 25 nM CLIP-170-1, and CP (0, 50, 100, or 500 nM). **(C)** Analysis of data in Fig. 2G & 2H, showing fold increase in actin filament elongation rates stimulated by 25 nM CLIP-170-1 in TIRF reactions containing 1 μM G-actin (10% OG-labeled; 0.2% biotin-actin), 5 μM profilin, 50 pM mDia1 (FH1-FH2-tail), and/or 25 nM CLIP-170-1, and/or 3 nM CP. Data averaged from three independent experiments (n = 100 filaments per condition in each experiment). Error bars, SE. **(D)** Average filament elongation rates measured from TIRF reactions; data are from reactions as in (C) above except with different CLIP-170-1 constructs, depicted in Figure 1H. Error bars, SE. **(E)** Average time to regrowth (n < 10) observed in TIRF movies as in Fig. 2G & 2H. Data only include events in which a filament barbed-end was initially capped for at least 20 s, and then subsequently resumed growth. Error bars, SE. Statistical differences: ns, not significantly different from control; a, compared to control (actin and profilin) (p < 0.05).

Figure S6.

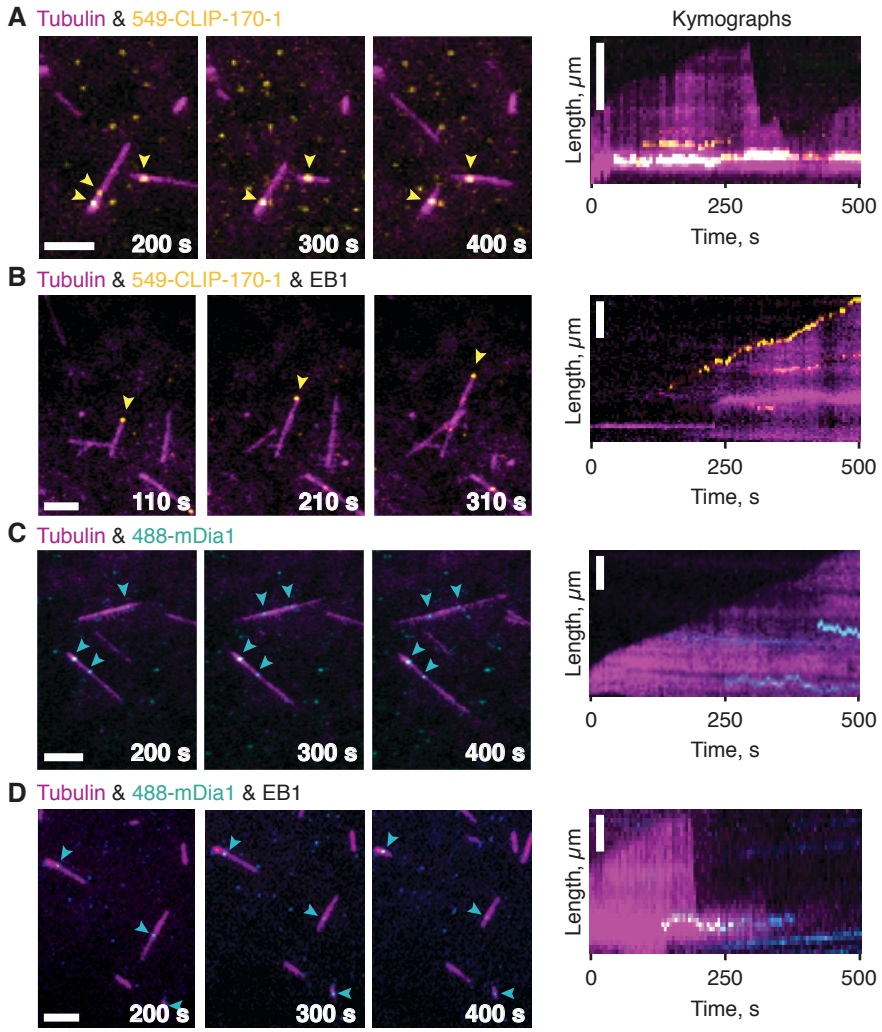

Fig. S6. Recruitment of CLIP-170-1 and mDia1 to MT sides and/or ends.
(A) Montage and kymographs showing that 549-CLIP-170 binds MT sides in the absence of EB1. **(B)** 549-CLIP-170 tracks MT plus ends in the presence of EB1. **(C-D)** 488-mDia1 binds MT sides in both the absence (C) and presence (D) of EB1. TIRF reactions contain: 15 µM tubulin (30% AlexaFluor649 labeled; biotinylated GMP-CPP MT seeds). Variable: 25 nM 549-CLIP-170-1, 100 pM 488-mDia1, 500 nM EB1. Scale bar, 5 µm.

Figure S7.

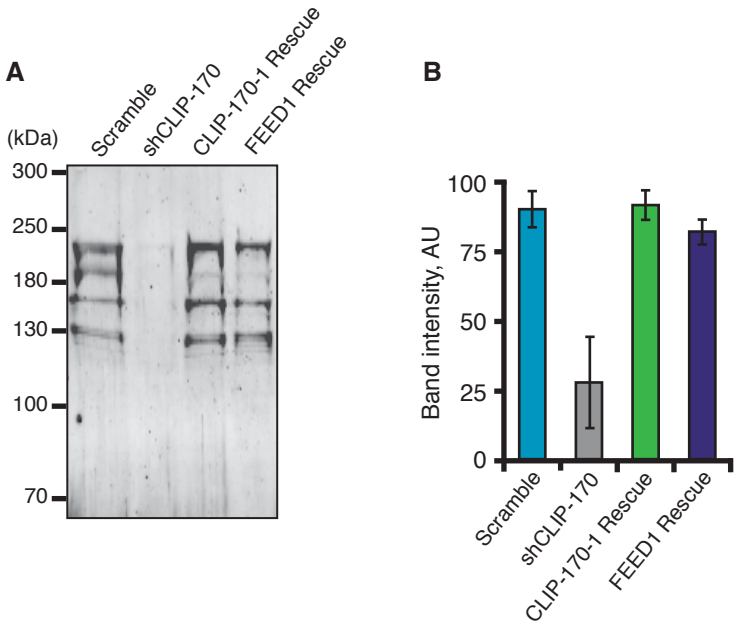

Fig. S7. Western blot analysis confirming shRNA knockdown of endogenous CLIP-170 proteins.
(A) N2A cells were transfected with a plasmid carrying an shRNA construct that targets all known isoforms of CLIP-170. Whole cell extracts were prepared after 48 h, fractionated on gels, transferred to membranes, and probed with a CLIP-170 antibody. **(B)** Band intensities were quantified; data are averaged from three separate experiments. Error bars, SD.

Figure S8.

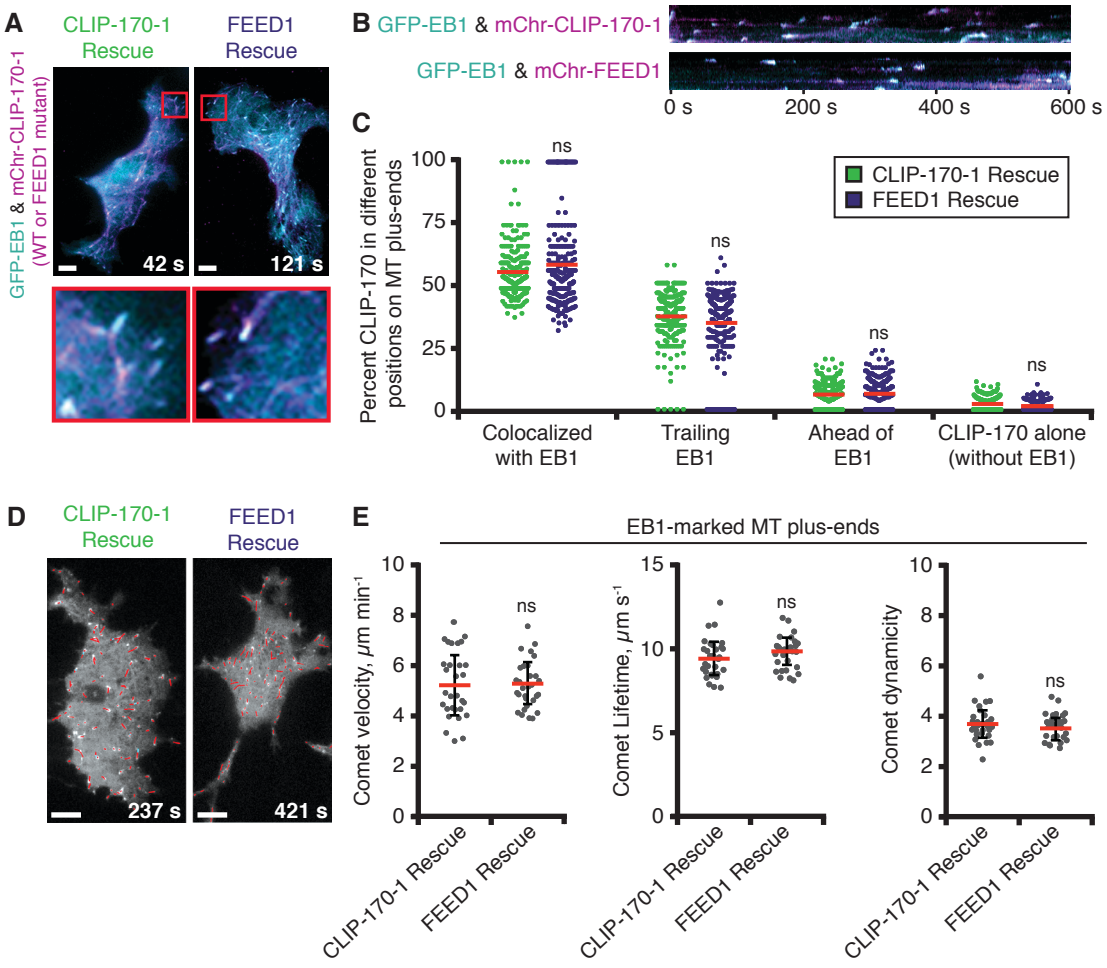

Fig. S8. MT localization and dynamics are not altered by FEED1 rescue.
(A) Localization of GFP-EB1 and mChr-CLIP-170 or mChr-FEED1 in N2A cells imaged by TIRF microscopy. Bar, 10 µm. Inset is 25 x 25 µm. **(B)** Kymographs showing the localization of EB1 or CLIP-170 construct at the periphery of N2A cells from movies in (A). **(C)** Percent of CLIP-170 colocalized with EB1 on MT plus-ends. 10 kymographs per treatment were scored for position on MT plus-ends from 30 cells (n = 300 kymographs per treatment). **(D-E)** Quantitative particle tracking of EB1 comets on growing MT plus-ends in CLIP-170 rescue or FEED1 rescue. **(D)** Images depiciting EB1 tracks in CLIP-170 or FEED1 rescue from utrack software. **(E)** Graphs show comet velocity, comet lifetime, and comet 'dynamicity' measured by utrack software (*36*). All utrack values were measured from $n \geq 30$ cells per condition.

Figure S9.

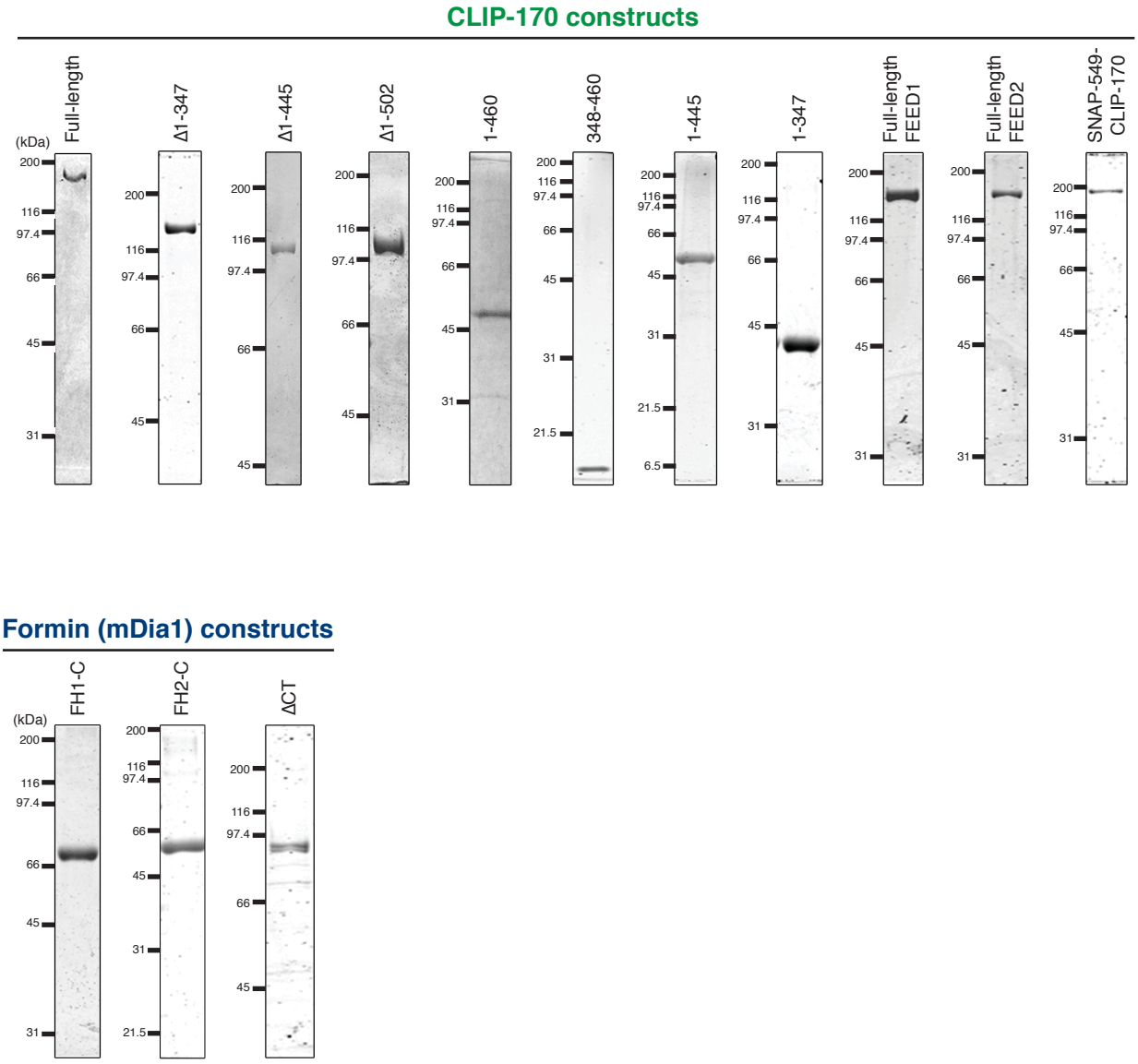

Fig. S9. Coomassie stained gels showing purified CLIP-170 and mDia1 polypeptides. SDS-PAGE gels of CLIP-170-1 polypeptides (full-length and fragments) and mDia1 polypeptides used in this study.

Movie S1. TIRF microscopy showing effects of mDia1 and/or CLIP-170-1 on actin filament assembly.
Reaction components: 1 μM G-actin (10% OG-labeled; 0.2% biotin-actin) and 5 μM profilin. Variable components: 25 nM full-length CLIP-170-1 and/or 50 pM mDia1 (FH1-FH2-tail). Video playback is 10 frames per s. Scale bar, 20 μm.

Movie S2. TIRF microscopy showing filaments polymerizing at different rates depending on the presence of mDia1 and/or CLIP-170-1.
Reaction components: 1 μM G-actin (10% OG-labeled; 0.2% biotin-actin), 5 μM profilin, 50 pM mDia1 (FH1-FH2-tail), and 25 nM full-length CLIP-170-1. Arrows highlight three filaments in a single field of view, each growing at a distinct rate. One filament grows slowly (~10 subunits s^{-1} μM^{-1}), at a rate consistent with a free barbed-end (white arrow). A second filament grows faster (~55 subunits s^{-1} μM^{-1}), at a rate consistent with mDia1-mediated stimulation (blue arrow). A third filament grows at an even faster or 'accelerated' rate (~180 subunits s^{-1} μM^{-1}), consistent with the combined effects of mDia1 and CLIP-170-1 (red arrow). Video playback is 10 frames per s. Scale bar, 20 μm.

Movie S3. Multi-wavelength single molecule TIRF microscopy comparing the effects of 649-mDia1 on actin filament elongation rate in the absence (left) and presence (right) of 549-CLIP-170-1.
Reaction components: 1 μM G-actin (10% OG-labeled; 0.2% biotin-actin), 5 μM profilin, and 50 pM 649-mDia1 (FH1-FH2-tail), with or without 25 nM 549-CLIP-170-1. Left panel shows a growing filament with 649-mDia1 on its barbed-end (purple arrows). Right panel shows a growing filament with 649-mDia1 and 549-CLIP-170-1 on its barbed-end (white arrows). Video playback is 10 frames per s. Scale bar, 10 μm.

Movie S4. Triple-color single molecule TIRF microscopy showing 649-mDia1 and 549-CLIP-170-1 tracking the barbed-end together and supporting accelerated actin filament elongation.
Reaction components: 1 μM G-actin (10% OG-labeled; 0.2% biotin-actin), 5 μM profilin, 50 pM 649-mDia1 (FH1-FH2-tail), and 25 nM 549-CLIP-170-1. Panels show individual channels and merge, as indicated. Video playback is 10 frames per s. Scale bar, 10 μm.

Movie S5. Multi-wavelength single molecule TIRF microscopy showing 549-CLIP-170-1 binding to the sides of microtubules and tracking microtubule plus ends in the absence (left) and presence (right) of EB1.
Reaction components: 15 μM tubulin (30% AlexaFluor649 labeled), biotinylated GMP-CPP MT seeds, 25 nM 549-CLIP-170-1, with or without 500 nM EB1. Video playback is 10 frames per s. Scale bar, 5 μm.

Movie S6. Triple-color single molecule TIRF microscopy showing the microtubule interactions of 488-mDia1 with or without 549-CLIP-170-1 in the presence or absence of EB1.
Reaction components: 15 μM tubulin (30% AlexaFluor649 labeled), biotinylated GMP-CPP MT seeds, and 100 pM 488-mDia1. Variable components: 25 nM 549-CLIP-170-1 and 500 nM EB1. Video playback is 10 frames per s. Scale bar, 5 μm.

Movie S7. Co-reconstitution and multi-wavelength TIRF microscopy of microtubules undergoing dynamic instability and actin filaments polymerizing in one reaction.
Reaction components: 15 μM tubulin (30% AlexaFluor649 labeled), biotinylated GMP-CPP MT seeds, and 1 μM G-actin (10% OG-labeled; 0.2% biotin-actin). Video playback is 10 frames per s. Scale bar, 5 μm.

Movie S8. Triple-color single molecule TIRF microscopy showing 549-CLIP-170-1 molecules being recruited to a microtubule plus end, and stimulating formation of two rapidly polymerizing actin filaments that remains attached to the microtubule surface.
Reaction components: 15 μM tubulin (30% AlexaFluor649 labeled), biotinylated GMP-CPP MT seeds, 1 μM G-actin (10% OG-labeled; 0.2% biotin-actin), 25 nM 549-CLIP-170-1, 100 pM mDia1, 5 μM profilin, and 500 nM EB1. Video playback is 10 frames per s. Scale bar, 5 μm.

Movie S9. Triple-color single molecule TIRF microscopy showing 549-mDia1 being recruited to a microtubule plus end, and stimulating formation of a rapidly polymerizing actin filament that remains attached to the microtubule surface.
Reaction components: 15 μM tubulin (30% AlexaFluor649 labeled), biotinylated GMP-CPP MT seeds, 1 μM G-actin (10% OG-labeled; 0.2% biotin-actin), 25 nM CLIP-170-1, 100 pM 549-mDia1, 5 μM profilin, and 500 nM EB1. Video playback is 10 frames per s. Scale bar, 5 μm.

Movie S10. Live imaging in N2A cells showing colocalization of GFP-EB1 and mChr-CLIP-170-1 (wild-type and FEED1 mutant).
N2A cells were depleted of endogenous CLIP-170 by expression of an shRNA construct, and rescued either with mChr-marked wild type or FEED1 mutant CLIP-170-1. Cells were co-transfected with a GFP-EB1 plasmid. Living cells were imaged by TIRF microscopy. GFP-EB1 comets shown in cyan; mChr-CLIP-170-1 comets shown in magenta. Images were acquired at 1 s intervals with 25 ms exposure times. Video playback is 25 frames per s. Scale bar, 10 μm.

Movie S11. Live imaging in N2A cells showing particle tracking of GFP-EB1 comets.
N2A cells were depleted of endogenous CLIP-170 by expression of an shRNA construct, and rescued either with mChr-marked wild type or FEED1 mutant CLIP-170-1. Cells were co-transfected with a GFP-EB1 plasmid. Living cells were imaged by TIRF microscopy. GFP-EB1 comets are shown in grayscale with MT trajectory particle tracking output overlaid as red lines. Images were acquired with 1 s intervals with 25 ms exposure times. Video playback is 25 frames per s. Scale bar, 10 μm.